Chemical Engineering Journal 417 (2021) 128080

Contents lists available at ScienceDirect

Chemical Engineering Journal

journal homepage: www.elsevier.com/locate/cej

Pressure drop and heat transfer of ZoneFlow™ structured catalytic reactors and reference pellets for Steam Methane Reforming

Florent Minette [a,b], Luis Calamote de Almeida [a,b,c], Sanjiv Ratan [c], Juray De Wilde [a,b,*]

[a] Université Catholique de Louvain, Materials & Process Engineering (IMAP), Place Sainte Barbe 2, B-1348 Louvain-la-Neuve, Belgium
[b] UCLouvain, Research and Innovation Centre for Process Engineering (ReCIPE), Place Sainte Barbe 2, B-1348 Louvain-la-Neuve, Belgium
[c] ZoneFlow Reactor Technologies, LLC, 41 Mechanic Street, P.O. Box 278, Windsor, CT 06095, USA

ARTICLE INFO

Keywords:
Structured catalytic reactors
Heat transfer
Pressure drop
Process intensification
Steam Methane Reforming

ABSTRACT

Structured catalytic reactors have the potential to combine reduced pressure drop and improved heat transfer compared to conventional pellets. In the present study, the pressure drop and heat transfer coefficient between the tube wall and the process gas were measured experimentally for annular structured ZoneFlow™ reactors of different design and for two commercial reference pellets. The ZoneFlow™ reactors differ by the design of the central rod that supports the near-wall annular casing. The experiments were carried out in a 1 m long reactor, at atmospheric pressure and with air flow rates from 70 to 330 Nm^3/h. To measure the heat transfer coefficient, the furnace was set at a constant temperature that was varied in the range 100–500 °C and the axial profiles of the tube wall and gas temperatures were measured. Using the experimental data, correlations for the friction factor and the Nusselt number were derived and the introduced parameters estimated using non-linear regression. A correlation for the static contribution to heat transfer for the structured reactors was derived from 3D numerical simulations. The correlations were then used to evaluate the pressure drop–heat transfer advantage of the structured reactors compared to the reference pellets at typical industrial steam methane reforming conditions. The data show that ZoneFlow™ reactors can provide a roughly doubled heat transfer coefficient at comparable pressure drop than the tested reference pellets. Furthermore, modification of the central rod support structure was found an efficient way to balance the pressure drop–heat transfer advantage of ZoneFlow™ reactors using an identical design casing.

1. Introduction

Steam reforming of natural gas is the most widely practiced process for the large-scale production of hydrogen and syngas, a mixture of hydrogen and carbon monoxide. Downstream applications include the production of ammonia, methanol, synthetic fuels via the Fischer–Tropsch synthesis and hydrotreatment processes, among others [1,2]. The conversion of natural gas to higher value products has recently gained interest, driven by the increased availability of natural gas, with impactful effects in terms of supply and price [3–8]. The expanding fertilizer market and related ammonia production is expected to increase hydrogen demand, as well as the increasing interest in methanol as flexible and transport efficient chemical intermediate. An increase in capacity and efficiency of steam methane reformers faces the limitations of the currently used reactor technology.

The reforming reactions are strongly endothermic and carried out in a multi-tubular fixed bed reactor, with hundreds of relatively small diameter tubes suspended in a furnace [9]. The throughput is limited by poor heat transfer between the tube inner wall and the process gas. Sufficient heat needs to be supplied without exceeding the maximum tube skin temperature. Around 50% of the total heat input to the reformer is effectively transferred to the process gas [10]. To prevent radial temperature differences and poor use of the catalyst in the center of a reformer tube, 10 cm diameter tubes are used [11–13]. To deal with as well constraints on pressure drop, interfacial transfer and intra-particle diffusion, complexly shaped and perforated pellets are used with an equivalent diameter of roughly 5–10 mm. Nevertheless, catalyst effectiveness factors lower than 5% are typically reported [14]. Pellets size and design can be optimized [15,16], but whatever their shape, there is a relatively well defined relation between heat transfer performance and pressure drop.

Structured catalytic reactors have been developed to deal with the limitations mentioned above and are of particular interest for highly exo- and endothermic reactions. An engineered packing is designed to optimize the flow pattern, in order to combine improved heat transfer

* Corresponding author at: Université Catholique de Louvain, Materials & Process Engineering (IMAP), Place Sainte Barbe 2, B-1348 Louvain-la-Neuve, Belgium.
E-mail address: juray.dewilde@uclouvain.be (J. De Wilde).

https://doi.org/10.1016/j.cej.2020.128080
Received 5 October 2020; Received in revised form 30 November 2020; Accepted 5 December 2020
Available online 13 December 2020

Nomenclature

$\mathcal{A}$	Cross-sectional area (m^2)
A	Heat exchanging surface (m^2)
a_v	Casing surface area per volume reactor ($m^2/m^3{}_r$)
C_A	Species molar concentration ($mol_A/m^3{}_g$)
c_p	Heat capacity at constant pressure (J/kg K)
d_{cat}	Catalyst coating thickness (m)
$\mathcal{D}_{eA}$	Effective diffusivity of species A in the catalyst coating ($m^3{}_g/m_{cat}.s$)
d_h	ZoneFlow™ hydraulic diameter (m)
d_p	Pellet diameter (m)
d_t	Tube diameter (m)
f	Friction factor
G	Gas mass flux ($kg_g/m^2{}_r.s$)
h	ZoneFlow™ casing material thickness (m)
ΔH	Heat of reaction (kJ/mol)
h_f	Heat transfer coefficient from gas to solid interface ($J/m^2{}_i$ K s)
k_g	Mass transfer coefficient from gas to solid interface ($m^3{}_g/m^2{}_i.s$)
L	ZoneFlow™ casing channel height (m)
Nu	Nusselt number
p	Total pressure (bar)
Pr	Prandtl number
q	Heat flux (W/m^2)
r_c	ZoneFlow™ reactor annulus width (m)
r_j	Rate of reaction j ($mol/kg_{cat}.s$)
Re	Reynolds number
T	Temperature (K)
u_s	Gas superficial velocity ($m^3{}_g/m^2{}_r.s$)
w	ZoneFlow™ casing channel width (m)
zz	Axial coordinate in the reactor (m)

Greek letters

$\alpha_{A,j}$	Stoechiometric coefficient of species A in reaction j
α_i	Convective heat transfer coefficient, bed side (W/m^2 K)
α^0	Static contribution to heat transfer (W/m^2 K)
ε	Reactor void fraction ($m^3{}_g/m^3{}_r$)
η_j	Effectiveness factor of reaction j
λ	Thermal conductivity (W/m K)
λ^0_{er}	Effective thermal conductivity in the radial direction (W/m K)
μ	Gas viscosity (Pa s)
ξ	Non-dimensional intra-catalyst coordinate
ρ_s	Catalyst density ($kg_{cat}/m^3{}_{cat}$)

Subscripts

d_h	ZoneFlow™ hydraulic diameter based
d_p	Particle diameter based
g	Gas phase
P	Reference pellets
s	Solid phase
t	Tube
w	Tube wall
ZF	ZoneFlow™ reactor

and reduced pressure drop compared to pellets. The use of a thin catalyst coating on the reactor internals ensures improved catalyst effectiveness. 3D printing technology has opened perspectives to new geometries, difficult to manufacture otherwise, but is still relatively expensive. Cost and ease of installation and replacement are important factors to account for when developing a structured reactor solution. Pangarkar et al. (2009) experimentally studied various structured packings, including open-cell foams, open cross flow (OCFS) and close cross flow (CCFS) structures, for the Fischer–Tropsch synthesis [17]. The combination of experimental measurements and fundamental modeling demonstrated better radial heat transport properties for these various structures compared to randomly packed beds, e.g. opening the way to operation with larger reactor diameters. Fratalocchi et al. (2018) carried out Fischer–Tropsch synthesis tests using an aluminum foam loaded with active $Co/Pt/Al_2O_3$ catalyst spheres of 300 μm diameter, under commercially representative operating conditions [18]. The concept of a packed foam was introduced to overcome the catalyst inventory issue [19,20]. A comparison was made with a randomly packed bed of identical catalyst spheres diluted with inert α-Al_2O_3 particles of identical size. The packed foam was shown to be stable during temperature ramping while runaway was observed with the packed bed of spheres, demonstrating highly improved radial heat transport properties by the presence of the metallic foam. Sanz et al. (2016) performed methanol steam reforming experiments on several types of metal monoliths of various cell density and catalyst content [21]. Accurate radial temperature profile measurements showed steeper gradients with decreasing cell density, resulting from a lower effective thermal conductivity of the structure. Computational Fluid Dynamics (CFD) simulations confirmed this observation. Specific structures such as the ZoneFlow™ and the Catacel™ reactors have been designed for steam methane reforming and tested at the pilot and commercial scales. The latter uses stacked fans made of triangular ducts, guiding radially the gas toward and away from the tube wall [22,23]. The gas impinging the heated wall allows improving heat transfer performance and pressure drop is reduced by 10%–20% compared to pellets. The long-term performance of the Catacel™ reactor was evaluated under typical commercial steam reforming operating conditions [24] and the structure was demonstrated to increase the tube lifetime, allowing lower maximum tube skin temperature than with pellets, for a given reactor operating temperature.

The present study focuses on the annular ZoneFlow™ reactor [25], shown in Fig. 1. The annular casing is made of sectors with blades guiding the flow either towards or away from the tube wall. Radial fins separate partially the sectors, except in the near-wall region where small openings allow flow in between adjacent sectors. The flow impinging the tube wall is accompanied by a local increase of turbulence due to rapid changes in velocity magnitude and direction in the near-wall region. This results in improved heat transfer between the process gas and the tube wall. De Wilde and Froment (2012) evaluated the resulting performance in SMR by means of Computational Fluid Dynamics (CFD) simulations on a 1 meter long ZoneFlow™ reactor [26]. The reactor comprised the annular casing and a central core composed of stacked, perforated and corrugated cones. Using detailed intrinsic kinetics [27], they showed that higher methane conversion or throughput than with a conventional packed bed could be achieved, taking advantage of intensified heat transfer and high catalyst effectiveness factors, and despite the lower catalyst inventory. They also showed improved heat transfer reduces risk of coke formation, opening perspectives for operation at lower steam-to-carbon ratio. In follow-up CFD work, it was shown that most of the flow and conversion took place in the near-wall annulus, allowing simplification of the central core design [28]. As will

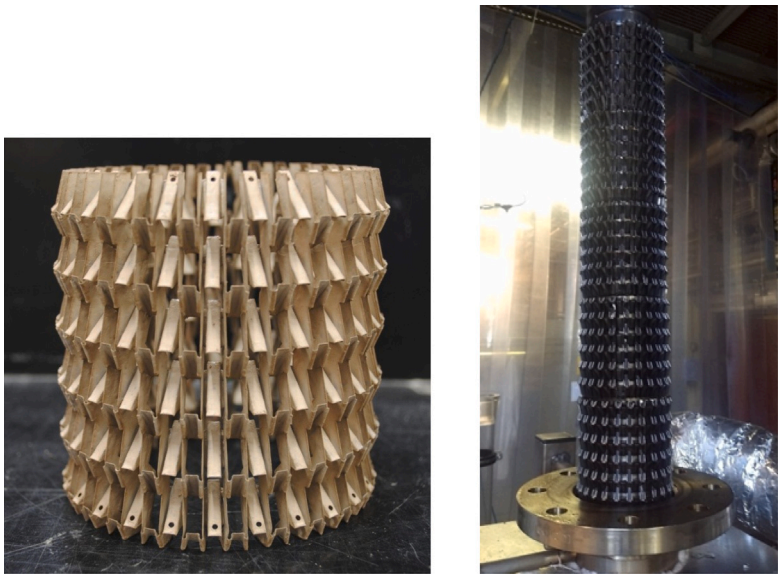

(a) (b)

Fig. 1. The near-wall annular ZoneFlow™ casing structure. (a) A single casing element consisting of six rows of blades and (b) five stacked casing elements.

be discussed in more detail later, the central core evolved to essentially a blocked tube equipped with collars or disks on which the annular casing is suspended. This suspension system is essential as it ensures close contact between the casing and the tube wall, the casing being pushed outward by its weight and the action of the flow. Additional CFD simulations were performed by De Wilde (2014) to study the effect of various design aspects of the casing, such as the blade angle of attack and the annulus width [29]. The annular ZoneFlow™ reactor can also be easily used with an open central tube (bayonet configuration) to allow counter-current heat recovery from the produced syngas that is directly used for the reforming, and reduce the excess steam produced downstream of the reformer - an aspect not studied further here.

In the present paper, the pressure drop and the heat transfer between the inner tube wall and the process gas are experimentally measured in a wide range of air flow rates, for various ZoneFlow™ reactors and for standard and low-pressure drop reference pellets. The influence of the annulus width and of the design of the casing-supporting central rod are studied and correlations for the friction factor and the Nusselt number are derived. Finally, using the derived correlations, a comparison of the heat transfer–pressure drop performance of the different reactors under typical commercial SMR conditions is made.

2. Experimental set-up

2.1. The ZoneFlow^{TM} reactors and reference pellets

The annular ZoneFlow™ casing is shown in Fig. 1(a). A casing element consists of 6 rows of blades and is 10 cm in length [25]. The annular casing is 11.5 mm wide (radially) and divided in 50 sectors (tangentially). The blades in the sectors make a 45° angle with the central axis and form channels that guide the flow either towards or away from the wall. Radial fins separate partially the sectors except in the near-wall region where flow between sectors is allowed through small openings. The channel height, L, the axial distance between two blades, is 17 mm. The average channel width, w, is the length of the circular arc between two adjacent radial fins midway (5.75 mm) from the wall and is 5.9 mm. The average hydraulic diameter of a ZoneFlow™ channel, or characteristic channel size, is then $d_h = 4\times(L\times w)/(2\times(L+w)) = 8.8$ mm. The casing is made of 100 μm thick stainless steel foil that is coated with catalyst. A 1 m long reactor containing 10 stacked casing elements is used. Fig. 1(b) shows 5 stacked casing elements mounted on the central rod prior to insertion in the tube. The reactor tube internal diameter is 10 cm, typical for conventional SMR. By the action of the flow, gravity and interaction with the collars or disks mounted on the central rod, the casing is pushed outward, ensuring good contact between the blades and the tube wall. Various designs of the central rod are considered in this study, as illustrated in Fig. 2. The ZF12-2C, ZF12-2D and ZF12-6D use a 7.6 cm diameter central rod, with corresponding annulus width r_c of 12 mm. The ZF12-2C design uses two conical collars per casing element (Fig. 2(a-b)). The ZF12-2D and ZF12-6D use respectively two and six disks per casing element (Fig. 2(c-f)). The collars and disks have an 86 mm external diameter. Compared to collars, disks are easier and less costly to manufacture. For the ZF12-2C and ZF12-2D designs, a gap in the near-central rod region exists in rows without collar or disk, allowing a certain gas by-pass. A lower pressure drop and, correspondingly, heat transfer coefficient is expected for such designs. The ZF14-2D86 and ZF14-2D84 designs use a 7.2 cm diameter central rod, providing a 14 mm annulus width. By adapting the outer diameter of the disks, an identical casing can be used in the 12 and 14 mm ZoneFlow™ reactors. Increasing the annulus width allows reducing the gas superficial velocity for a given flow rate, leading to reduced pressure drop. All ZF14 designs use two disks per casing element (Fig. 2(c-d)), but the disk size was varied with respectively an 86 and 84 mm external diameter. All the dimensions and design parameters are summarized in Table 1.

Identical pressure drop and heat transfer testing is carried out using standard and low-pressure drop reference pellets. The standard pellets are quadralobe with 4 holes and a 5.9 mm equivalent diameter, defined as the diameter of the sphere with the same surface area per unit volume. The low-pressure drop reference pellets are cylinders with 7 holes and an 8.6 mm equivalent diameter. The pellets dimensions, densities and measured bed void fractions are summarized in Table 2.

2.2. Operating conditions and instrumentation

The pressure drop and heat transfer coefficient between the tube wall and the process gas are experimentally measured in the setup shown in Fig. 3(a). A schematic representation is given in Fig. 3(b). Air is fed at different flow rates between 60 and 330 Nm^3/h, covering mass

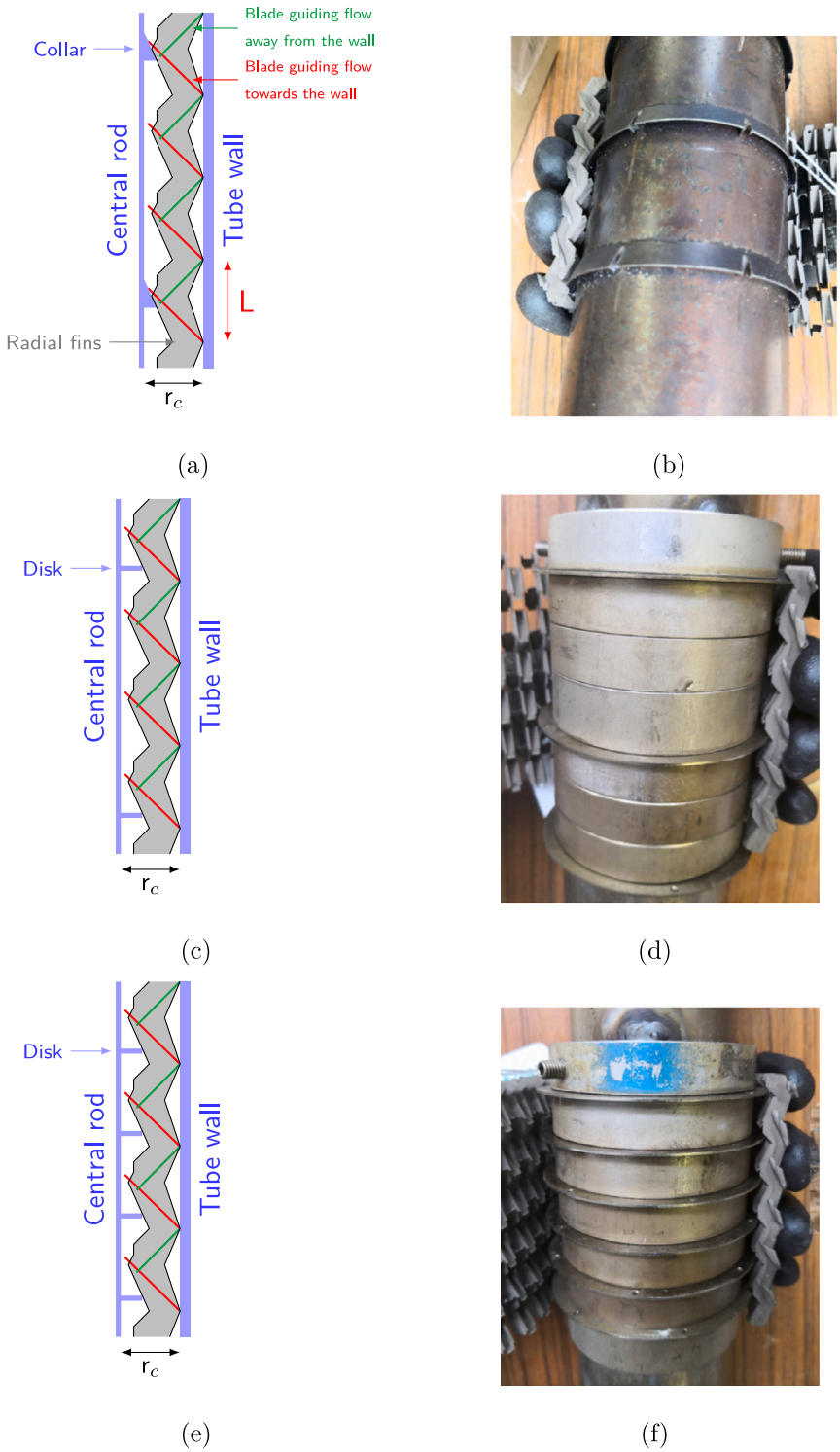

Fig. 2. Schematic representation and picture of the ZoneFlow™ structure with a central rod comprising (a)–(b) 2 conical collars per casing elements (ZFxx-2C), (c)–(d) 2 disks per casing element (ZFxx-2D) and (e)–(f) 6 disks per casing element (ZFxx-6D).

Table 1
The various ZoneFlow™ reactors considered in this study.

	ZF12-2C	ZF12-2D	ZF12-6D	ZF14-2D86	ZF14-2D84
Annulus width, r_c (mm)	12	12	12	14	14
Central rod diameter (mm)	76	76	76	72	72
Central rod configuration (per casing element)	2 collars	2 disks	6 disks	2 disks	2 disks
Disk/collar diameter (mm)	86	86	86	86	84
Casing specific surface area a_v (m^2/m_r^3)	397	397	397	340	340
Void fraction, ε (m_g^3/m_r^3)	0.98015	0.98015	0.98015	0.983	0.983

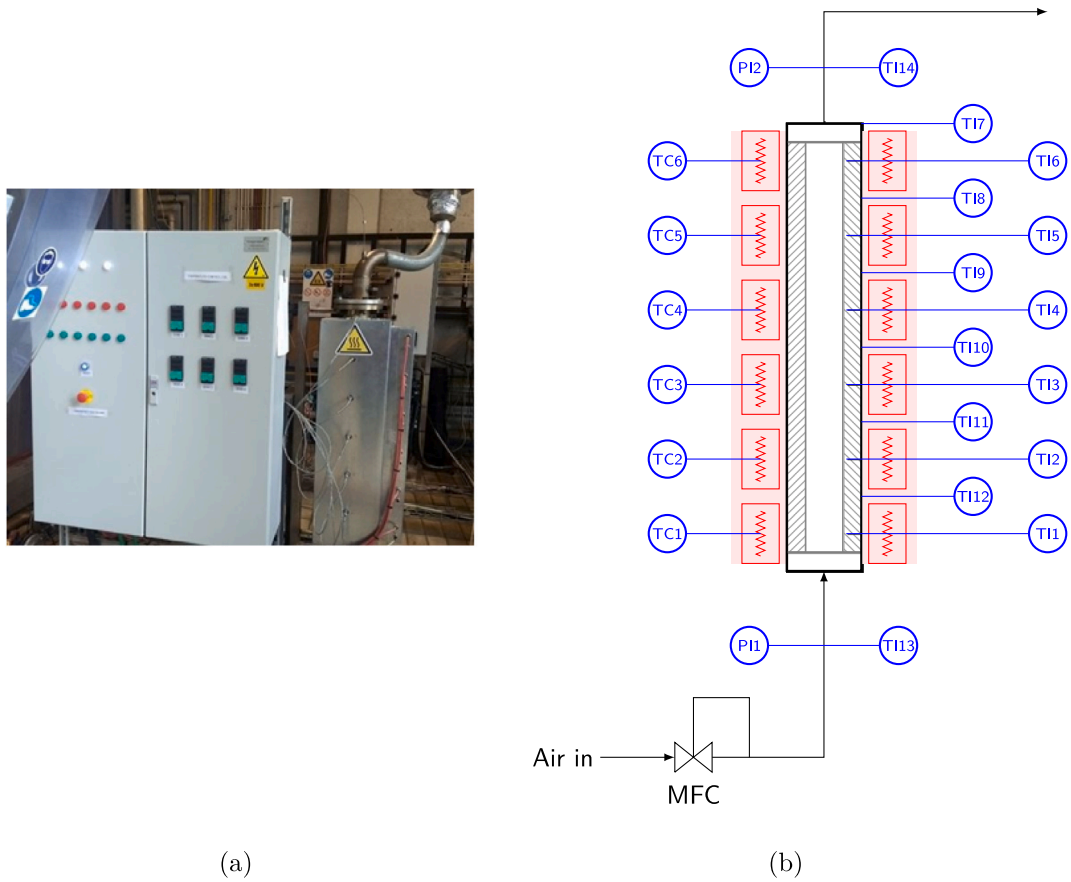

Fig. 3. (a) Picture and (b) schematic representation of the experimental setup for pressure drop and heat transfer measurements. MFC: Mass flow controller, PI: pressure indicator, TI: temperature indicator, TC: temperature indicator and controller.

Table 2
Properties and dimensions of the tested reference pellets.

	Standard reference pellets	Low-dP reference pellets
		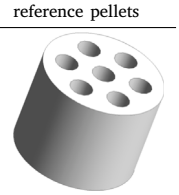
Equivalent diameter, d_p (cm)	0.59	0.86
Pellet material density, ρ_s (kg_{cat}/m^3_{cat})	2365	1455
Bed density, ρ_b (kg_{cat}/m^3_r	1058	556.3
Bed void fraction, ε (m^3_g/m^3_r)	0.55	0.62

Table 3
Simulated conditions for numerical evaluation of the so-called static contribution to heat transfer in the ZoneFlow™ structure.

Gas thermal conductivity	λ_g (W/m K)	0.0242, 0.04, 0.055
Solid thermal conductivity	λ_s (W/m K)	5, 15, 25, 35, 45
Casing material thickness	h (μm)	50, 100, 150

flow rates typical for commercial SMR. Atmospheric pressure is imposed at the exit of the reactor. For the ZoneFlow™ reactor with 12 mm annulus width, the channel hydraulic diameter-based Reynolds number ranges between 3620 and 17100, and for the ZoneFlow™ reactor with 14 mm annulus width, between 3150 and 14900. For the reference packed bed reactors, the particle diameter-based Reynolds numbers for the standard and low-dP pellets range between 1000 and 4800 and between 1500 and 7000 respectively. In commercial steam reformers, depending on the downstream applications, applied particle diameter-based Reynolds numbers typically range between 2000 and 7500 [1,2,14]. This range is well covered by the experimental conditions in this study. The pressure is measured right upstream and downstream the reactor by two GE Druck DPI 800 series pressure indicators PI1 and PI2, operating in the range 0–3000 mbarg, with accuracy of ± 5 mbar. The insulated furnace contains six 18 cm long heating blocks whose the temperature is independently set using PID controllers and measured by thermocouples TC1-TC6. The temperature of the heating blocks is imposed constant. Five different temperatures are used: 100, 200, 300, 400 and 500 °C. The inlet and outlet gas temperatures are measured by thermocouples TI13 and TI14. The process gas and tube wall temperatures are measured at 6 axial positions, by the thermocouples TI1-TI6 and TI7-TI12 respectively. The tube wall thickness is 4 mm and thermocouples TI7-TI12 are cemented 2 mm deep into the tube wall to have them properly shielded from radiation from the furnace elements. With the ZoneFlow™ reactors, the gas thermocouples TI1-TI6 are placed at around 3 mm radial distance from the central rod. CFD simulations [26,28] showed excellent radial temperature uniformity in ZoneFlow™ reactors, the flow continuously being forced to move radially towards or away from the tube wall. For tests with pellets, the thermocouples inserted into the bed are protected by an open-ended thermowell and positioned at 1.6 cm from the tube wall, where the average temperature is expected. All used thermocouples are K-type with a 1.5 mm OD and an accuracy of ± 2.2 °C.

Table 4
Correlations for the friction factors and the Nusselt numbers for the two reference pellets and the 5 tested ZoneFlow™ configurations.

		Friction factor for pressure drop		Nusselt number for heat transfer	
Reference pellets	Standard pellets	$f = 10.5\frac{(1-\varepsilon)^{1.2}}{\varepsilon^3}Re_{d_p}^{-0.3}$	$R^2_{adj} = 0.967$	$Nu_{d_p} = \frac{\alpha_p^0 d_p}{\lambda_g} + 0.25Re_{d_p}^{0.72}Pr^{1/3}$	$R^2_{adj} = 0.963$
	Low-dP pellets	$f = 4.63\frac{(1-\varepsilon)^{1.2}}{\varepsilon^3}Re_{d_p}^{-0.16}$	$R^2_{adj} = 0.985$	$Nu_{d_p} = \frac{\alpha_p^0 d_p}{\lambda_g} + 0.15Re_{d_p}^{0.76}Pr^{1/3}$	$R^2_{adj} = 0.968$
ZoneFlow^{TM} structure	ZF12-2C	$f = \frac{16}{Re_{d_h}} + 0.272Re_{d_h}^{-0.05}$	$R^2_{adj} = 0.988$	$Nu_{d_h} = \frac{\alpha_{ZF}^0 d_h}{\lambda_g} + 8.34Re_{d_h}^{0.36}Pr^{1/3}$	$R^2_{adj} = 0.979$
	ZF12-2D	$f = \frac{16}{Re_{d_h}} + 0.331Re_{d_h}^{-0.06}$	$R^2_{adj} = 0.989$	$Nu_{d_h} = \frac{\alpha_{ZF}^0 d_h}{\lambda_g} + 4.27Re_{d_h}^{0.43}Pr^{1/3}$	$R^2_{adj} = 0.979$
	ZF12-6D	$f = \frac{16}{Re_{d_h}} + 0.569Re_{d_h}^{-0.06}$	$R^2_{adj} = 0.989$	$Nu_{d_h} = \frac{\alpha_{ZF}^0 d_h}{\lambda_g} + 4.85Re_{d_h}^{0.43}Pr^{1/3}$	$R^2_{adj} = 0.977$
	ZF14-2D86	$f = \frac{16}{Re_{d_h}} + 0.468Re_{d_h}^{-0.07}$	$R^2_{adj} = 0.995$	$Nu_{d_h} = \frac{\alpha_{ZF}^0 d_h}{\lambda_g} + 5.75Re_{d_h}^{0.41}Pr^{1/3}$	$R^2_{adj} = 0.954$
	ZF14-2D84	$f = \frac{16}{Re_{d_h}} + 0.401Re_{d_h}^{-0.07}$	$R^2_{adj} = 0.98$	$Nu_{d_h} = \frac{\alpha_{ZF}^0 d_h}{\lambda_g} + 5.38Re_{d_h}^{0.41}Pr^{1/3}$	$R^2_{adj} = 0.969$

Table 5
Considered air and SMR mixture properties and operating conditions for evaluation and comparison of the heat transfer coefficient for the ZoneFlow™ reactors and the reference pellets (see Figs. 10 and 11).

Air Fig. 10(a)		Typical SMR mixture Fig. 10(b)	
T	300 °C	T	700 °C
p	1 bar	p	30 bar
μ	3.0×10^{-5} Pa s	μ	3.0×10^{-5} Pa s
c_p	1027 J/kg K	c_p	2450 J/kg K
λ_g	0.044 W/m K	λ_g	0.0735 W/m K
Pr	0.7	Pr	1
Composition (mol.%)		*Composition (mol.%)*	
O_2	21	CH_4	20
N_2	79	H_2O	60
		H_2	10
		CO_2	5
		CO	2.5
		N_2	2.5

3. Modeling and parameter estimation

3.1. Pressure drop

The pressure drop in the ZoneFlow™ reactor can be calculated by means of a Fanning-type equation:

$$\frac{dp}{dz} = -2f\frac{\rho_g u_s^2}{d_h} \tag{1}$$

Based on an analogy with a bundle of empty channels with hydraulic diameter d_h, the friction factor, f, is modeled by:

$$f = \frac{16}{Re_{d_h}} + a_1 Re_{d_h}^{-a_2} \tag{2}$$

with the first term the well-known friction factor for laminar flow in empty tubes, but using the Reynolds number based on the hydraulic diameter of a single ZoneFlow™ channel, $Re_{d_h} = Gd_h/\mu$, and the second term of a similar functional form as reported for turbulent flow in empty tubes with 5000 < Re < 200000 ($f = 0.046Re_D^{-0.2}$) [30]. The empirical parameters a_1 and a_2 in Eq. (2) are to be estimated by regression for each tested configuration.

For the pellets, the pressure drop can be calculated as:

$$\frac{dp}{dz} = -f\frac{\rho_g u_s^2}{d_p} \tag{3}$$

The friction factor f is modeled using the relation introduced by Hicks (1970) [31]:

$$f = a_3\frac{(1-\varepsilon)^{1.2}}{\varepsilon^3}Re_{d_p}^{-a_4} \tag{4}$$

with the equivalent diameter-based Reynolds number $Re_{d_p} = Gd_p/\mu$. Hicks (1970) [31] determined for randomly packed spherical particles that a_3 = 6.8 and a_4 = -0.2, but the parameters a_3 and a_4 were re-estimated for the complexly shaped reference pellets that were tested. Note that the classical Ergun equation [32] is only valid when $Re_{d_p}/(1-\varepsilon) < 500$, whereas the Handley and Hegg's equation is valid for $1000 < Re_{d_p}/(1-\varepsilon) < 5000$. The present study covers the range $2200 < Re_{d_p}/(1-\varepsilon) < 18400$. Hicks (1970) proposed Eq. (4) that fits Ergun's (1952) [32] and Handley and Hegg's (1968) [33] data, as well as the results of Wentz and Thodos at very high Reynolds number [30,34] and is therefore adopted here. The pressure drop Eqs. (1) and (3), for the ZoneFlow™ and pellets reactors respectively, were integrated using a 4th order Runge–Kutta method. The variations of air density and viscosity with pressure and temperature were accounted for using the ideal gas law and Sutherland's relation. During the pressure drop tests, the measured temperature difference between the inlet and outlet air did not exceed 10 °C and a mean constant temperature was considered. The parameters a_1-a_4 were estimated using non-linear least squares regression. The objective function to be minimized is given by:

$$\text{SSQ} = \sum_{i=1}^{n}\left(\Delta P_i - \widehat{\Delta P}_i\right)^2 \xrightarrow{a} \min \tag{5}$$

where ΔP_i and $\widehat{\Delta P}_i$ are the measured and predicted pressure drop measured for the ith experiment. The software Athena Visual Studio was used for the parameter estimation.

3.2. Heat transfer modeling

A standard correlation for the ZoneFlow™ hydraulic diameter based Nusselt number is proposed for the ZoneFlow™ reactors:

$$Nu_{d_h} = \frac{\alpha_i d_h}{\lambda_g} = \frac{\alpha_{ZF}^0 d_h}{\lambda_g} + b_1 Re_{d_h}^{b_2} Pr^{1/3} \tag{6}$$

with b_1 and b_2 empirical parameters to be estimated from experimental data for each tested configuration. α_i is the heat transfer coefficient for convective heat transfer between the tube wall and the process gas, as introduced in 1D reactor models [30]. Note that the use of a 1D reactor model is particularly justified for ZoneFlow™ reactors with the process gas forced to continuously flow towards and away from the wall. This leads to excellent radial temperature uniformity as it was illustrated by CFD simulations [26,28]. A similar approach based on 1D reactor modeling was adopted by Giani et al. (2005) to derive a correlation for the Nusselt number to describe the gas–solid heat transfer in open-celled metallic foams [35]. The calculation of the so-called static contribution in the ZoneFlow™ structure α_{ZF}^0 is addressed numerically, as explained below. Because of the very high void fraction of ZoneFlow™ reactors (> 0.98), a comparison with the heat transfer coefficient of empty tubes is worth making. In the classical Dittus–Boelter equation, b_1 = 0.023 and b_2 = 0.8, the so-called static contribution being negligible.

For the pellets, a similar correlation for the Nusselt number based on the equivalent diameter is adopted:

$$Nu_{d_p} = \frac{\alpha_i d_p}{\lambda_g} = \frac{\alpha_P^0 d_p}{\lambda_g} + b_3 Re_{d_p}^{b_4} Pr^{1/3} \tag{7}$$

The so-called static contribution α_P^0 is given by [36,37]:

$$\alpha_P^0 = \frac{10.21\lambda_{er,p}^0}{d_t^{4/3}} \tag{8}$$

The effective radial thermal conductivity $\lambda_{er,p}^0$ is calculated using the relation introduced by Kunii and Smith (1960) [38]. Some authors also investigated heat transfer parameters in fixed bed reactors theoretically and using CFD simulations [39,40].

To estimate parameters b_1-b_4, non-linear regression is performed between measured and calculated gas temperatures at different axial positions. The objective function to be minimized is given by:

$$\text{SSQ} = \sum_{i=1}^{n}\sum_{k=1}^{6} w_{ik}\left(T_{g,ik} - \hat{T}_{g,ik}\right)^2 \xrightarrow{\boldsymbol{b}} \min \tag{9}$$

with $T_{g,ik}$ and $\hat{T}_{g,ik}$ the measured and predicted temperatures for the ith experiment at the axial position corresponding to the kth thermocouple (TI1-TI6). Weighted regression was applied with w_{ik} the weight given to a certain data point. The gas temperatures at a given axial position is calculated by integrating the following continuity equation:

$$u_s \rho_g c_p \frac{dT_g}{dz} = A_b\left(\frac{1}{\alpha_i} + \frac{e}{\lambda_w}\frac{A_b}{A_m}\right)^{-1}\left(T_w - T_g\right) \tag{10}$$

where T_g is the calculated axial profile of the process gas temperature and T_w is the measured axial profile of the tube wall temperature, imposed during the regression. Thermal conduction in the tube wall is accounted for, with e the tube thickness and λ_w the thermal conductivity of the tube material, i.e. stainless steel. Note that since the tube thermocouples TI7-TI12 are cemented 2 mm deep in the 4 mm thick tube wall, e is taken to be 2 mm. A_b is the heat exchanging surface between the gas and the tube wall on the inner tube side. A_m is the log mean of A_b and A_t, with A_t the heat exchanging surface at the radial position of the wall thermocouples TI7-TI12. The contribution of radiative heat transfer between the tube wall and the reactor internals was found negligible in the range of temperatures experimentally tested and absorption of radiation by air can be neglected. In certain experiments with pellets, some thermocouples were displaced when loading the bed and were contacting the tube wall, which was confirmed by means of additional and repetitive experiments. Gas temperature measurements were then falsified at these axial positions and the corresponding data were given zero weight. The parameter estimation was performed using the software Athena Visual Studio.

The so-called static, or conductive, contribution was found to be very small compared to the dynamic or convective contribution in the window of flow rates tested. A statistically significant estimation of parameter α_{ZF}^0 from experimental data is then not feasible, but important in order to be able to determine the parameters of the dynamic contribution with sufficient precision. This static contribution was therefore estimated numerically using finite volume simulations. The steady-state Laplacian equation, Eq. (11), was solved in a virtually reconstructed ZoneFlow™ structure containing 3 rows of blades and 4 sectors, as shown in Fig. 4:

$$\nabla\left(\lambda_{er,ZF}^0 \nabla T\right) = 0 \tag{11}$$

A temperature difference ΔT of 25 K was imposed between the two boundaries of the domain in the radial direction and adiabatic conditions were imposed at all other surfaces. The static effective radial thermal conductivity in the ZoneFlow™ structure $\lambda_{er,ZF}^0$ is then evaluated via:

$$\lambda_{er,ZF}^0 = \frac{r_c \int_{\mathcal{A}} q\, d\mathcal{A}}{\mathcal{A}\Delta T} \tag{12}$$

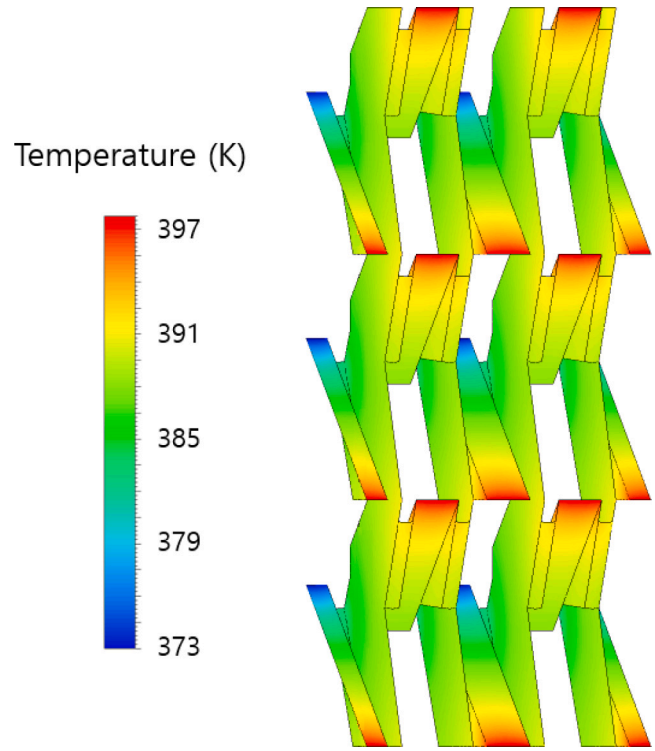

Fig. 4. Computational domain for the numerical evaluation of the so-called static contribution in the ZoneFlow™ structure and contour plot of temperature for λ_g = 0.0242 W/m K, λ_s = 25 W/m K and a casing material thickness of 100 μm.

with q the calculated heat flux, $\mathcal{A}$ the cross-sectional area in the radial direction and r_c the width of the computational domain. The so-called static contribution for the ZoneFlow™ structure to the heat transfer coefficient then follows from:

$$\alpha_{ZF}^0 = \frac{\lambda_{er,ZF}^0}{r_c} \tag{13}$$

To derive a correlation for α_{ZF}^0 as a function of the gas and casing properties, the thermal conductivity of the gas and of the casing material were varied and simulations were repeated for different casing thickness. The simulated conditions are summarized in Table 3. The finite volume solver Fluent 18.1 (Ansys) was used with a second order upwind discretization scheme for the Laplacian operator. Convergence was supposed to be achieved for residuals below 10^{-16}. The approach is similar to that adopted by Bracconi et al. (2018) to study the influence of geometrical properties on the effective thermal conductivity of open-cell foams [41].

4. Results and discussion

4.1. Friction factors and pressure drop

The correlations for the friction factors with optimal estimates of the empirical parameters are given in Table 4, for both reference pellets and the various ZoneFlow™ reactors. The fit between experimental data and correlations is evaluated via the adjusted R-squared value. Fig. 5 illustrates the good fit between the measured and predicted pressure gradient as a function of the air flow rate, for all tested configurations. The standard reference pellets exhibit a 70% higher pressure drop than the low-dP pellets. ZoneFlow™ reactors with disks or collars (ZF12-2D and ZF12-2C) offer a relatively similar pressure drop, with a slightly lower pressure drop with the profiled collars. All ZoneFlow™ reactors except the ZF12-6D offer lower pressure drop than

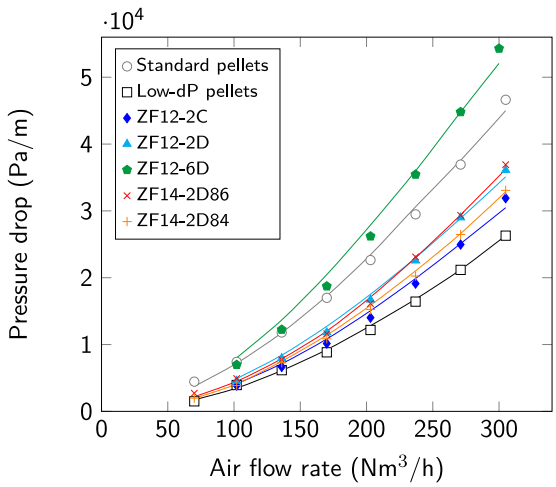

Fig. 5. Pressure drop versus air flow rate for the ZoneFlow™ reactors and reference pellets. Points: experimental data, lines: predicted by model.

the standard reference pellets. The ZF14-2D86 exhibits a very similar pressure drop than the ZF12-2D while the ZF14-2D84 exhibits a similar pressure drop than the ZF12-2C. At same flow rate, a comparable but slightly higher pressure drop than with the low-dP pellets is achieved with the ZF12-2C and ZF14-2D84.

The values of the parameters a_1 and a_2 (Table 4) in the correlation for the turbulent contribution to the friction factor in ZoneFlow™ reactors, Eq. (2), and comparison with the values for an empty tube show that a_1 is significantly higher than in an empty tube, whereas exponent a_2 is clearly smaller. The forced radial motion of the flow in the ZoneFlow™ casing channels and in sectors, guiding the flow towards and away from the tube wall, and the motion in between sectors via relatively narrow gaps results in clearly different pressure drop behavior compared to empty tubes. Comparing the values of the parameters a_3 and a_4 in the correlation for the friction factor of the reference pellets, Eq. (4), with the values for spherical particles obtained by Hicks (1970) [31], it is clear that with the standard reference pellets – which aim at high heat transfer – both a_3 and exponent a_4 are somewhat higher, whereas with the low pressure drop reference pellets, both a_3 and a_4 are somewhat lower.

4.2. Static contribution to heat transfer

For the static contribution to heat transfer in the ZoneFlow™ reactors, the effective radial thermal conductivity is described using a thermal resistances model. In absence of flow and if radiation is not accounted for, the mechanisms contributing to static effective conduction are the following:

(a) Conduction in the gas phase
(b) Conduction in the stagnant film in the vicinity of the contact surface between the ZoneFlow™ casing and the tube wall
(c) Conduction in the solid phase

The combination of the different contributions, depending on whether they operate in series or parallel (see Fig. 6(a)), leads to the following equation for the static effective thermal conductivity:

$$\frac{\lambda^0_{er,ZF}}{\lambda_g} = \varepsilon + \frac{(1-\varepsilon)}{\beta + \gamma \frac{\lambda_g}{\lambda_s}} \tag{14}$$

with β and γ parameters to be estimated by regression using the numerically generated data. Eq. (14) is similar to the model proposed by Kunii and Smith (1960) [38] for a fixed bed reactor. Note that

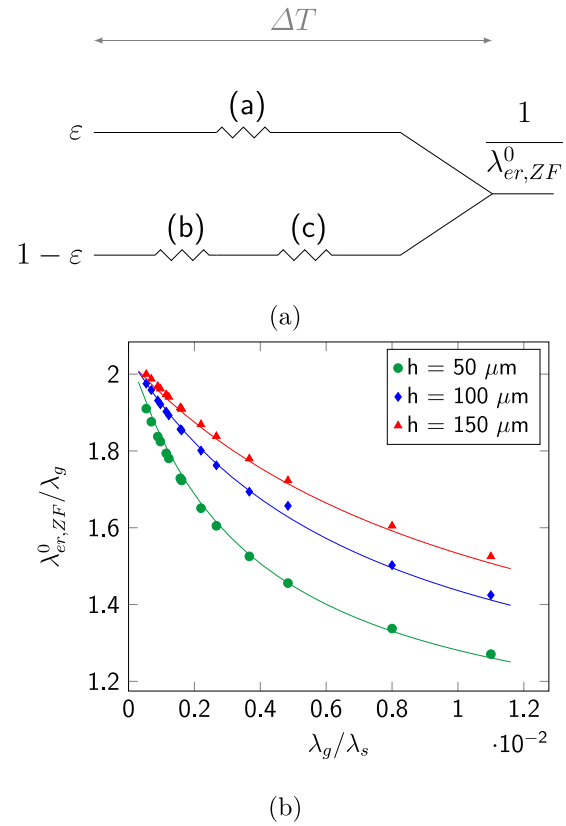

Fig. 6. (a) Resistances model for the static effective radial thermal conductivity in the ZoneFlow™ reactor. (b) Static effective radial thermal conductivity in the ZoneFlow™ structure: comparison between the numerically generated data and the resistances model (Eq. (15)). Symbols: generated data, lines: model.

the void fraction ε is very high in ZoneFlow™ reactors ($\varepsilon = 0.98015$ for the ZF12-2C, ZF12-2D and ZF12-6D and $\varepsilon = 0.983$ for the ZF14-2D86 and ZF12-2D84) and is given by $1 - a_v/2 \times h$. β was found to be proportional to the casing material thickness and is given by $\beta = 212 \times h$. The parameter γ was found to be constant with value of 2.82. The static effective radial conductivity in the ZoneFlow™ structure can then calculated according to:

$$\frac{\lambda^0_{er,ZF}}{\lambda_g} = \varepsilon + \frac{(1-\varepsilon)}{212h + 2.82\frac{\lambda_g}{\lambda_s}} \tag{15}$$

The fit between the numerically generated data and Eq. (15) is shown in Fig. 6(b). Thermal conduction in the solid phase does not contribute significantly as the void fraction is high (> 0.98) and thermal conduction is strongly limited by gas phase conduction. Consequently, selecting a highly conductive casing material will hardly increase the value of $\lambda^0_{er,ZF}$. Compared to open-cells foams for example, the static effective radial thermal conductivity in the ZoneFlow™ structure is around one order of magnitude smaller, when a solid material with identical thermal conductivity is used. Indeed, Bracconi et al. (2018) [41] showed that for a typical open-cell foam with porosity of 0.9, the static effective radial thermal conductivity is around $0.04 \times \lambda_s$. Note that the ZoneFlow™ structure is typically made of stainless steel, with a thermal conductivity of around 25 W/m K. Open-cells foams are usually made of aluminum, with thermal conductivity around one order of magnitude higher. The static effective radial thermal conductivity of such open-cells foams will then be two orders of magnitude higher than that of ZoneFlow™ reactors. This confirms that thermal conduction in the internals of a ZoneFlow™ reactor has a minor contribution to the overall heat transfer, as assumed in the CFD simulations by De Wilde

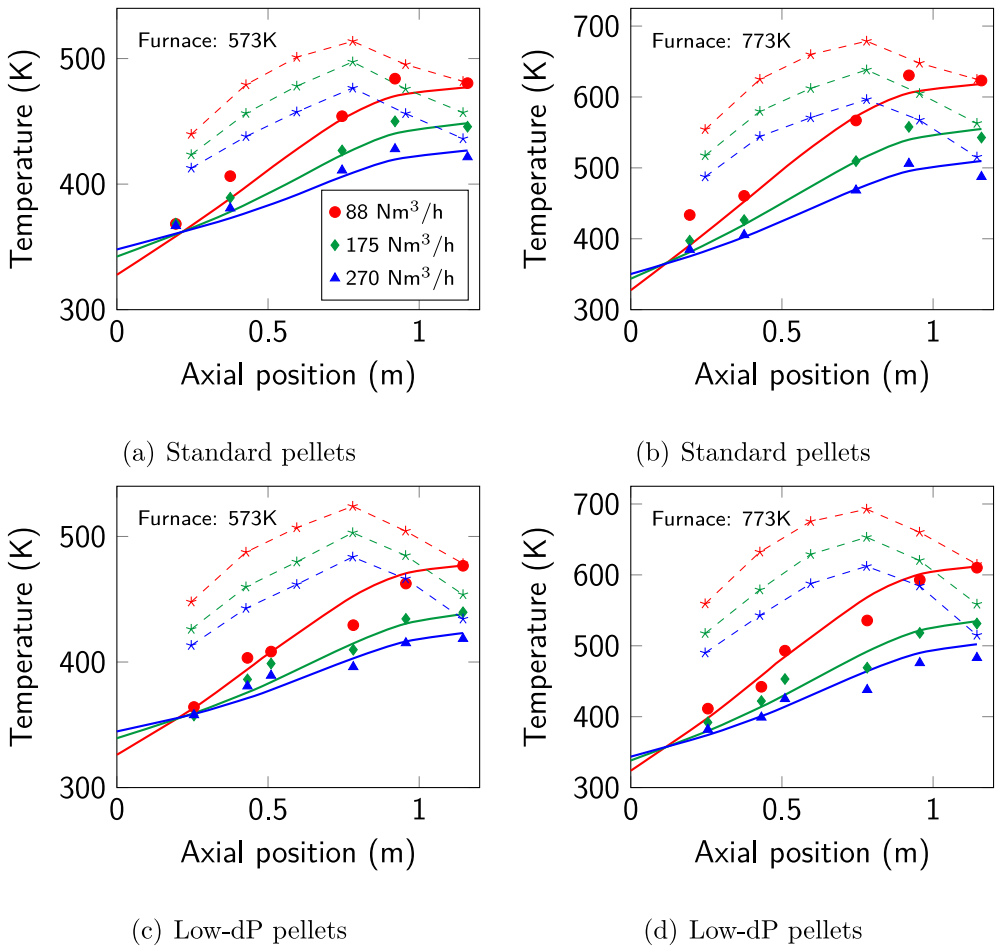

Fig. 7. Measured and predicted axial air temperature profiles for the standard and low-dP reference pellets, for three applied flow rates and two furnace temperatures. Symbols: experimental gas temperature, solid lines: predicted by model, dashed lines: experimental tube wall temperature.

and Froment [26,28]. This is not surprising for a high void fraction (> 0.98) structured packing in stainless steel. Whether this could be a limitation for application with e.g. highly exothermic reactions is to be further studied, but the dynamic contribution makes the overall heat transfer highly efficient as discussed hereafter.

4.3. Dynamic contribution to heat transfer

Table 4 summarizes the Nusselt number correlations for the reference pellets and the ZoneFlow™ reactors with optimal estimates for the parameters b_1-b_4. The static contributions α^0_P and α^0_{ZF} were calculated using Eqs. (8), (13) and (15). The quality of the fit is reflected in the adjusted R-squared values. Figs. 7–9 compare the measured and predicted air temperature profiles, for the different pellets and ZoneFlow™ reactors tested. The measured tube wall temperature profiles, imposed for the regression are also shown. The profiles are shown for three of the applied air flow rates (88, 175 and 270 Nm^3/h) and two of the imposed furnace temperatures (573 and 773 K). For the standard reference the pellets, the temperature value measured by the second thermocouple (TI2) is not shown, as the latter was detected to touch the tube wall and was not accounted for in the regression. Note that the air inlet temperature is not identical in all tests. The improved heat transfer of the ZoneFlow™ reactors compared to the pellets can be visually observed in Figs. 7–9 from the more rapid increase of the air temperature and the more pronounced difference in air temperature between the air inlet and outlet, on the one hand, and the smaller temperature differences between the tube wall and the air, the driving force for the heat transfer, on the other hand.

Comparing the values of the parameters b_1 and b_2 (Table 4) in the heat transfer correlations for the ZoneFlow™ reactors, Eq. (6), with the values for an empty tube (Dittus–Boelter equation) shows that b_1 is significantly higher (more than two orders of magnitude), while exponent b_2 is about half of the value for an empty tube. This is similar to what was observed for the parameter values of the friction factor, see Section 4.1, and indicates that a clearly different heat transfer performance compared to an empty tube is introduced by the ZoneFlow™ flow pattern. For the pellets, the parameter values b_3 and b_4 obtained with both reference pellets indicate that heat transfer is mostly limited by wall heat transfer, and to less extent by effective radial conduction in the bed. Aerov and Umnik (1951), for example, reported $Nu_w = 0.155 Re^{0.75} Pr^{1/3}$, Li and Finlayson (1977) reported $Nu_w = 0.17 Re^{0.79}$ for $20 < Re_p < 7600$, with values of b_3 and b_4 close to those derived in this work [42,43]. Note that all experiments were done with air, so $Pr^{1/3} \simeq 0.89$. In case radial effective conductivity also limits heat transfer, values of exponent b_4 in the correlation for the overall Nusselt number are typically higher — de Wasch and Froment (1972) derived $b_4 = 1$, Li and Finlayson (1977) report $b_4 = 0.95$ [37,43].

Fig. 10(a) shows the heat transfer coefficient α_i between the tube wall and the gas as a function of the flow rate (in Nm^3/h), using the correlations shown in Table 4, for the two reference pellets and the different ZoneFlow™ reactors and for typically tested operating conditions, i.e. air at atmospheric pressure and 300 °C. The considered physico-chemical properties of air are summarized in Table 5. For the pellets, α^0_P = 70 and 75 W/m^2 K for the standard and low-dP reference pellets respectively. For the ZoneFlow™ reactors, α^0_{ZF} = 6.4 W/m^2 K for the ZF12-2C, ZF12-2D and ZF12-6D and 5.1 W/m^2 K for the ZF14-2D86 and ZF14-2D84, confirming that static effective radial thermal

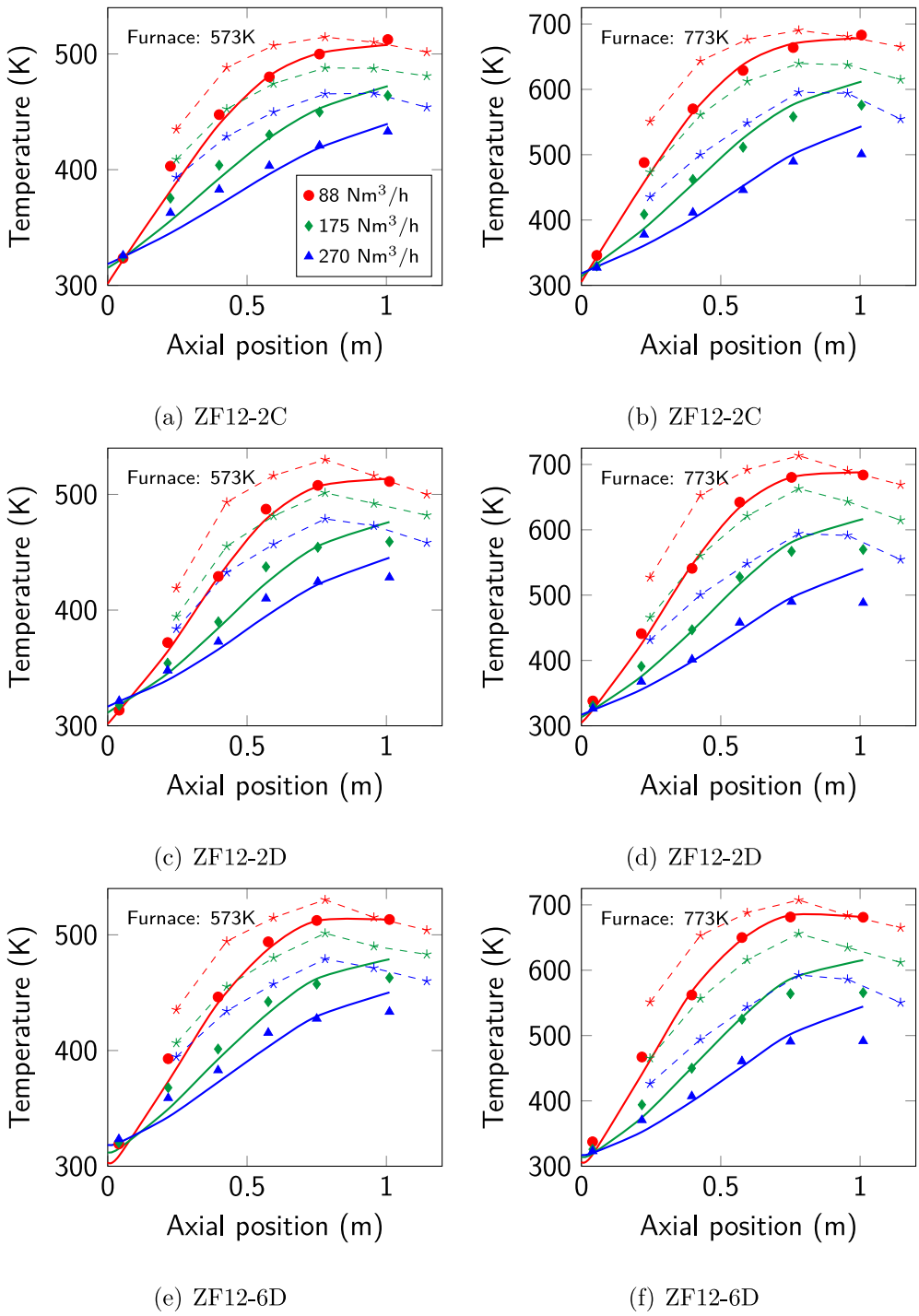

Fig. 8. Measured and predicted axial air temperature profiles for the ZF12-2C, ZF12-2D and ZF12-6D, for three applied flow rates and two furnace temperatures. Symbols: experimental gas temperature, solid lines: predicted by model, dashed lines: experimental tube wall temperature.

conductivity is a minor contribution to the heat transfer in ZoneFlow™ reactors. As expected, the standard reference pellets offer a somewhat better heat transfer than the low-dP pellets. A much more improved heat transfer is observed with the ZoneFlow™ reactors, for which α_i is about 2 times higher than for the low-dP pellets, with a pressure drop in between that of the standard and low-dP reference pellets, except for the ZF12-6C. The latter offers significantly higher values of α_i, but at the cost of a higher pressure drop than the other ZoneFlow™ reactors, as seen in Fig. 5. Logically, the ZoneFlow™ reactors with higher heat transfer coefficient have a higher pressure drop as well. The relation heat coefficient–pressure drop is, however, different than with the pellets as will be illustrated hereafter. Note that with pellets, the increase of α_i with the air flow rate is gradual. In contrast, ZoneFlow™ reactors exhibit a rapid increase of α_i with air flow rate at low flow rates, after which the increase becomes more gradual. This is explained by the rapid local generation of turbulence in the near-wall region where the flow is forced to abruptly change direction. This is a distinct feature of ZoneFlow™ reactors that was already observed in CFD simulations [26,28,29]. Fig. 10(b) shows the extrapolated values of the heat transfer coefficient at typical steam reforming operating conditions. The considered operating conditions and physico-chemical properties of the SMR mixture are also summarized in Table 5. The

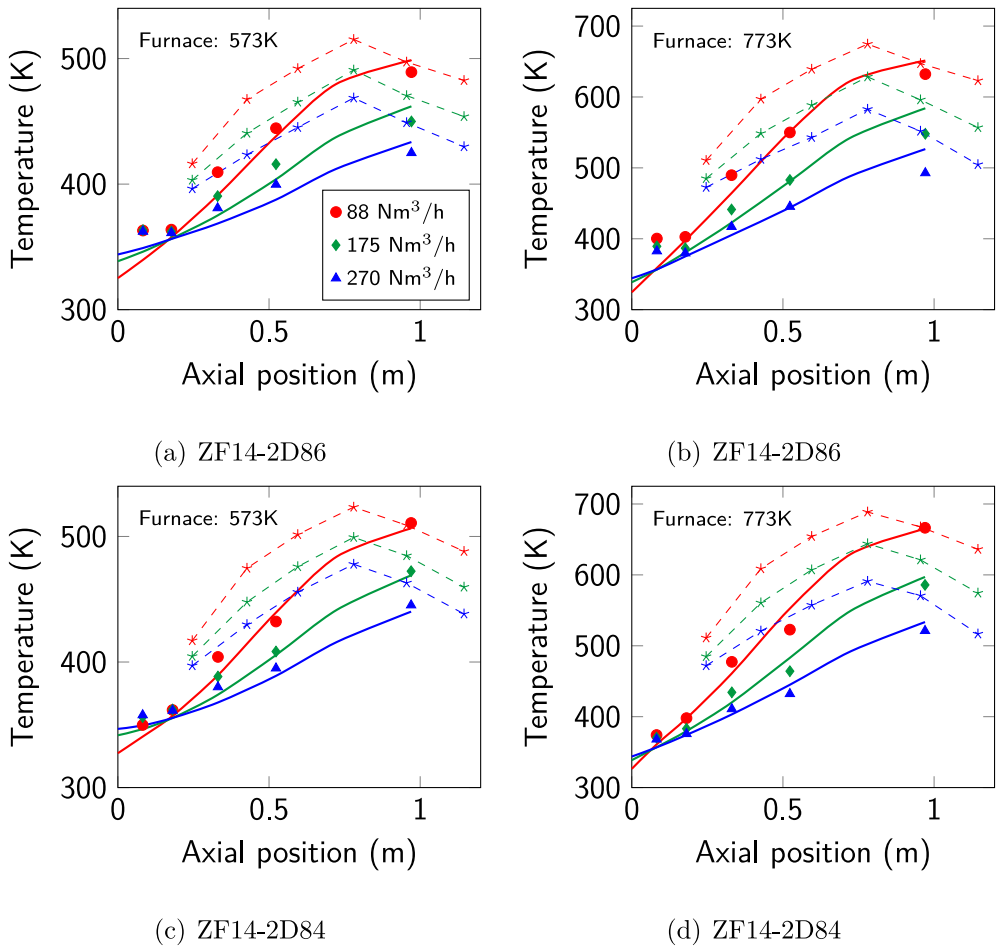

Fig. 9. Measured and predicted axial air temperature profiles for the ZF14-2D86, ZF14-2D84, for three applied flow rates and two furnace temperatures. Symbols: experimental gas temperature, solid lines: predicted by model, dashed lines: experimental tube wall temperature.

exact same trends are observed. Under these conditions, radiation is also expected to play a significant role in ZoneFlow™ reactors [26,28] ensuring even better heat transfer performance compared to pellets.

The diagram in Fig. 11 illustrates the relative heat transfer coefficient versus the relative pressure drop for the standard pellets and the ZoneFlow™ reactors. Performance is compared to the reference low-dP pellets. The open symbols are for typically tested conditions, with an air flow rate of 175 Nm^3/h (see Fig. 10(a)). The filled symbols are for typical steam reforming operating conditions with a flow rate of 500 Nm^3/h (see Fig. 10(b)). The physico-chemical properties are identical to those used in Fig. 10 and reported in Table 5. The standard reference pellets provide a heat transfer coefficient approximately 25%–30% higher than that of low-dP pellets, but with a pressure drop that is approximately 90% higher. The ZF12-2C and ZF12-2D have similar but slightly higher pressure drop, respectively 10 and 25%, than the low-dP reference pellets, but the heat transfer coefficient is slightly more than doubled compared to the latter. The ZF14-2D84 and ZF14-2D86 provide very similar pressure drop than the ZF12-2C and ZF12-2D respectively, with the heat transfer coefficient also slightly more than doubled compared to the low-dP reference pellets. The ZF12-6D provides even better heat transfer, but the pressure drop is around 2 times higher than that of the low-dP pellets and around 1.1 times higher compared to the standard reference pellets. This does not necessarily mean that the integral or overall pressure drop over a ZF12-6D reactor will be higher than that with pellets. This depends on the length of the reactor and, for given throughput, improved heat transfer allows to shorten the reactor provided a sufficiently active catalyst is used. Fig. 12 illustrates again the different relation between heat transfer and pressure drop for the ZoneFlow™ reactors than for pellets. The graph clearly shows that at equivalent pressure drop, heat transfer two to three times more efficient can be achieved with the ZoneFlow™ reactors compared to the reference pellets.

5. Conclusions

The pressure drop and heat transfer performance of annular ZoneFlow™ reactors of different designs and of standard and low-pressure drop reference pellets was experimentally studied and correlations for the friction factor, the heat transfer coefficient and their parameters derived from experimental data. The ZoneFlow™ reactor designs vary by the annulus width and the number of collars or disks that are mounted on the central rod to suspend the annular structured casing. Measurements were carried out with air at atmospheric pressure and in a wide air flow rate range. The pressure drop in the ZoneFlow™ reactor is well described by the Fanning-type equation. With the reference pellets, the relation of Hicks (1970) gave a good fit with re-estimated parameters. Heat transfer measurements were performed using a constant furnace temperature which was varied between 100 and 500 °C. The process gas and tube wall temperature were measured at six axial positions. The latter were imposed in the regression. Standard correlations for the Nusselt number with optimized parameter values were capable of reproducing the measured axial air temperature profiles. For the ZoneFlow™ reactors, a resistance-type model for the static contribution to heat transfer had to be first derived from 3D numerical simulations. These confirm that thermal conduction in the solid internals has a minor contribution to the overall heat transfer in ZoneFlow™ reactors, which by design have a very high void fraction.

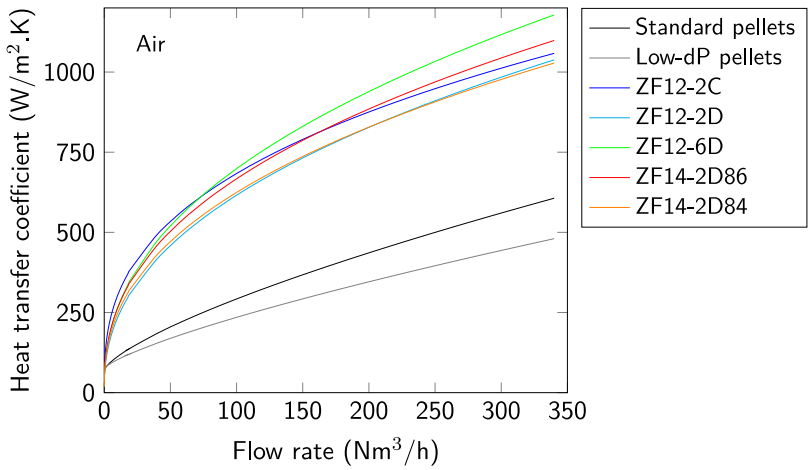

(a)

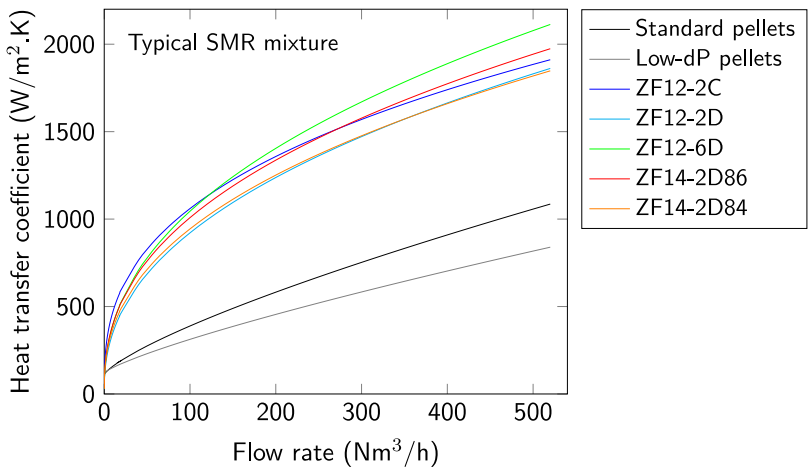

(b)

Fig. 10. Comparison of the predicted heat transfer coefficients α_i versus flow rate for the reference pellets and the ZoneFlow™ reactors using the derived correlations, for (a) typically tested operating conditions (flow of air at 300 °C and atmospheric pressure) and typically commercially applied SMR operating conditions (30 bar and 700 °C). See Table 5 for the considered physico-chemical properties.

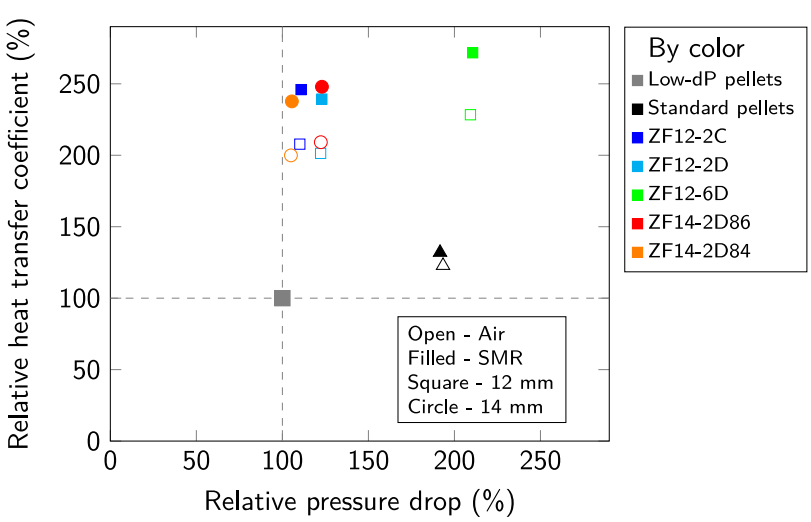

Fig. 11. Relative heat transfer coefficient versus relative pressure drop of the ZoneFlow™ reactors and the standard pellets compared to the low-dP pellets. Open symbols: typical experimentally tested conditions (air at atmospheric pressure and 300 °C) at a flow rate of 175 Nm^3/h, filled symbols: typical commercially applied SMR conditions (SMR mixture at 30 bar and 700 °C) at a flow rate of 500 Nm^3/h. See Table 5 for the physico-chemical properties.

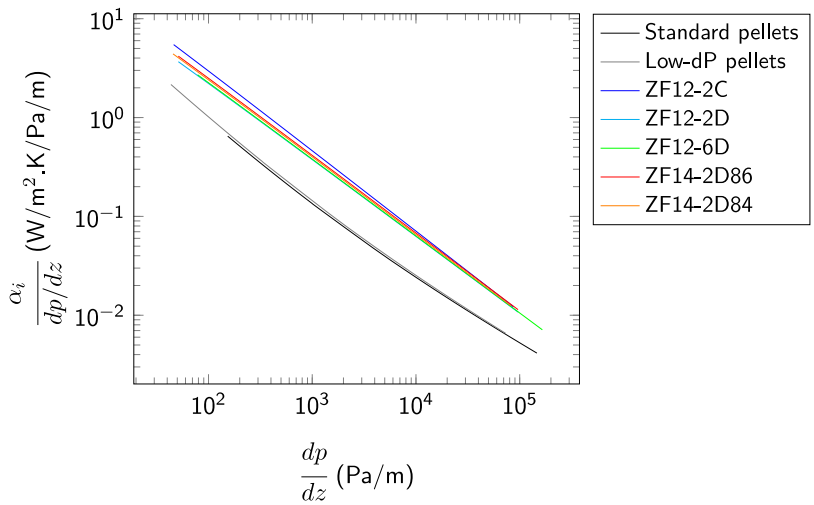

Fig. 12. Predicted relationship pressure drop versus heat transfer for the reference pellets and the ZoneFlow™ reactors, for typically tested operating conditions: flow of air at 300 °C and atmospheric pressure and flow rate between 5 and 340 Nm^3/h. See Table 5 for the considered physico-chemical properties.

The data and analysis have shown that ZoneFlow™ reactors offer a distinct advantage when comparing the heat transfer–pressure drop relation to that of conventional pellets and that modifying the number of collars or disks that suspend the annular structured casing, or the annulus width, are efficient ways to vary the heat transfer versus pressure drop advantage. Conical collars or easier to manufacture disks provide a very similar effect on heat transfer and pressure drop. By adapting their outer diameter, an identical casing can be used in the 12 mm and 14 mm-annulus width ZoneFlow™ reactors. Most ZoneFlow™ reactors tested offer a circa 100% increased heat transfer coefficient compared to the low-dP reference pellets, with a pressure drop between that of low-dP and standard reference pellets. The ZoneFlow™ design with the 12 mm annulus and 6 disks per casing element offers an even higher increase of the heat transfer coefficient, at the cost of a pressure drop that is about 100% higher than that of the standard reference pellets, but shortening the reactor could be considered.

Declaration of competing interest

One or more of the authors of this paper have disclosed potential or pertinent conflicts of interest, which may include receipt of payment, either direct or indirect, institutional support, or association with an entity in the biomedical field which may be perceived to have potential conflict of interest with this work. For full disclosure statements refer to https://doi.org/10.1016/j.cej.2020.128080.The authors would like to thank ZoneFlow Reactor Technologies for the financial support of the research project.

Acknowledgments

This research was financed by ZoneFlow™ Reactor Technologies, LLC. Computational resources have been provided by the Consortium des Équipements de Calcul Intensif (CECI), funded by the Fonds de la Recherche Scientifique de Belgique (F.R.S-FNRS), Belgium under Grant No. 2.5020.11 and by the Walloon Region, Belgium.

References

[1] J.A. Moulijn, M. Makkee, A. Van Diepen, Chemical Process Technology, John Wiley & Sons Ltd, Chichester, 2001.
[2] C.H. Bartholomew, R.J. Farrauto, Fundamentals of Industrial Catalytic Processes, second ed., John Wiley & Sons, INC., Hoboken, New Jersey, 2006.
[3] W.E. Liss, Impacts of shale gas advancements on natural gas utilisation in the United States, Energy Tehcnol. 2 (2014) 953–967.
[4] W. Liss, Demand Outlook: a golden age of natural gas, Chem. Eng. Prog. 108 (2012) 35–40.
[5] E. McFarland, Unconventional chemistry for unconventional natural gas, Science 338 (2012) 341–342.
[6] R.S. Middleton, R. Gupta, J.D. Hyman, H.S. Viswanathan, The shale gas revolution: Barriers, sustainability, and emerging opportunities, Appl. Energy 199 (2017) 88–95.
[7] V. Arora, Y. Cai, U.S. natural gas exports and their global impacts, Appl. Energy 120 (2014) 95–103.
[8] M. Melikoglu, Shale gas: Analysis of its role in the global energy market, Renew. Sust. Energ. Rev. 37 (2014) 460–468.
[9] I. Dybkjaer, K. Aasberg-Petersen, Synthesis gas technology: Large-scale applications, Can. J. Chem. Eng. 94 (2016) 607–612.
[10] J.R. Rostrup-Nielsen, J. Sehested, Steam reforming for hydrogen the process and the mechanism, Fuel Chem. Div. Prepr. 48 (2003) 218–219.
[11] M.N. Perdernera, J. Pina, D.O. Borio, V. Bucala, Use of a heterogeneous two-dimensional model to improve the primary steam reformer performance, Chem. Eng. J. 94 (2003) 29–40.
[12] A.G. Dixon, Local transport and reaction rates in a fixed bed reactor tube: Endothermic steam methane reforming, Chem. Eng. Sci. 168 (2017) 156–177.
[13] A.G. Dixon, Fixed bed catalytic reactor modelling: the radial heat transfer problem, Can. J. Chem. Eng. 90 (2012) 507–527.
[14] Xu, G.F. Froment, Methane steam limitations and reforming: II. Diffusional reactor simulation, AIChE J. 35 (1989) 97–103.
[15] J.R.H. Ross, Large-scale catalytic reactors, in: Heterogeneous Catalysis, 2012, pp. 143–169.
[16] A.G. Dixon, M.E. Taskin, M. Nijemeisland, E.H. Stitt, Wall-to-particle heat transfer in steam reformer tubes: CFD comparison of catalyst particles, Chem. Eng. Sci. 63 (2008) 2219–2224.
[17] K. Pangarkar, T.J. Schildhauer, J.R. van Ommen, J. Nijenhuis, J.A. Moulijn, F. Kapteijn, Experimental and numerical comparison of structured packings with a randomly packed bed reactor for Fischer–Tropsch synthesis, Catal. Today 147S (2009) S2–S9.
[18] L. Fratalocchi, C.G. Visconti, G. Groppi, L. Lietti, E. Tronconi, Intensifying heat transfer in Fischer–Tropsch tubular reactors through the adoption of conductive packed foams, Chem. Eng. J. 349 (2018) 829–837.
[19] D. Vervloet, F. Kapteijn, J. Nijenhuis, J.R. van Ommen, Process intensification of tubular reactors: Considerations on catalyst hold-up of structured packings, Catal. Today 216 (2013) 111–116.
[20] C.G. Visconti, G. Groppi, E. Tronconi, Highly conductive packed foams: A new concept for the intensification of strongly endo- and exo-thermic catalytic processes in compact tubular reactors, Catal. Today 273 (2016) 178–186.
[21] O. Sanz, I. Velasco, I. Reyero, I. Legorburu, G. Arzamendi, L.M. Gandia, M. Montes, Effect of the thermal conductivity of metallic monoliths on methanol steam reforming, Catal. Today 273 (2016) 131–139.
[22] Johnson Matthey buys Catacel, to grow steam methane reforming, Fuel Cells Bull. (Issue 10) (2014) 9–10.
[23] M. Basin, D. Gary, W. Whittenberger, J. Shah, Increased steam methane reformer throughput: Switching to a foil based catalyst technology raised throughput substantially for a hydrogen producer, 2017, https://www.catacel.com.
[24] W. Whittenberger, Permanent, high performance, drop-in replacement catalyst for steam reforming hydrogen plants, 2010, https://www.catacel.com.
[25] ZoneFlow™ Reactor Technologies, LLC - catalyst for steam methane reforming, 2007, https://www.zoneflowtech.com.

[26] J. De Wilde, G.F. Froment, Computational fluid dynamics in chemical reactor analysis and design: Application to the ZoneFlow™ reactor for methane steam reforming, Fuel 100 (2012) 48–56.
[27] J. Xu, G.F. Froment, Methane steam reforming methanation and water-gas shift: I. Intrinsic kinetics, AIChE J. 35 (1989) 88–96.
[28] J. De Wilde, G.F. Froment, Modeling of dual-zone structured reactors for natural gas steam reforming, Ind. Eng. Chem. Res. 52 (2013) 14055–14065.
[29] J. De Wilde, High heat transfer low pressure drop structured catalytic reactors for steam methane reforming, in: 14th AIChE Annual Meeting, Atlanta, GA, USA, November 2014, pp. 16-21.
[30] G.F. Froment, K.B. Bischoff, J. De Wilde, Chemical Reactor Analysis and Design, third ed., Wiley, 2010.
[31] R.E. Hicks, Pressure drop in packed beds of spheres, Ind. Eng. Chem. Fundam. 9 (1970) 500–502.
[32] S. Ergun, Fluid flow through packed columns, Chem. Eng. Prog. 48 (1952) 89–94.
[33] D. Handley, P.J. Heggs, Momentum and heat transfer mechanisms in regular shaped packings, Trans. Inst. Chem. Eng. (1968) T251.
[34] C.A. Wentz Jr, G. Thodos, Pressure drops in the flow of gases through packed and distended beds of spherical particles, AIChE J. 9 (1963) 81–84.
[35] L. Giani, G. Groppi, E. Tronconi, Heat transfer characterization of metallic foams, Ind. Eng. Chem. Res. 44 (2005) 9078–9085.
[36] A.P. de Wasch, G.F. Froment, A two dimensional heterogeneous model for fixed bed catalytic reactors, Chem. Eng. Sci. 26 (1971) 629–634.
[37] A.P. de Wasch, G.F. Froment, Heat transfer in packed beds, Chem. Eng. Sci. 27 (1972) 567–576.
[38] D. Kunii, J.M. Smith, Heat transfer characteristics of porous rocks, AIChE J. 6 (1960) 71–78.
[39] A.G. Dixon, D.L. Cresswell, Theoretical prediction of effective heat transfer parameters in packed beds, AIChE J. 25 (1979) 663–676.
[40] A.G. Dixon, M. Nijemeisland, CFD as a design tool for fixed-bed reactors, Ind. Eng. Chem. Res. 40 (2001) 5246–5254.
[41] M. Bracconi, M. Ambrosetti, M. Maestri, G. Groppi, E. Tronconi, A fundamental analysis of the influence of the geometrical properties on the effective thermal conductivity of open-cell foams, Chem. Eng. Process. 129 (2018) 181–189.
[42] M.E. Aerov, N.N. Umnik, Heat transfer from the tubes with packed beds, Zhurnal Tech. Phiziki 21 (1951) 1364–1371.
[43] C.-H. Li, B.A. Finlayson, Heat transfer in packed beds - a reevaluation, Chem. Eng. Sci. 32 (1977) 1055–1066.